Nitrogen-Doped Carbon Quantum Dots on Graphene for Field-Effect Transistor Optoelectronic Memories †

Mahima Chaudhary, Chenghao Xin, Zhelu Hu, Dongjiu Zhang, Guillaume Radtke, Xiangzhen Xu, Laurent Billot, Charlotte Tripon-Canseliet, Zhuoying Chen

Nitrogen-Doped Carbon Quantum Dots on Graphene for Field-Effect Transistor Optoelectronic Memories[†]

Mahima Chaudhary,[1] Chenghao Xin,[1] Zhelu Hu,[1] Dongjiu Zhang,[1] Guillaume Radtke,[2] Xiangzhen Xu,[1] Laurent Billot,[1] Charlotte Tripon-Canseliet[1] and Zhuoying Chen[1,*]

[1.] LPEM, ESPCI Paris, PSL Research University, Sorbonne Université, CNRS, 10 Rue Vauquelin, F-75005 Paris, France

[2.] Sorbonne Université, Muséum National d'Histoire Naturelle, UMR CNRS 7590, IRD, Institut de Minéralogie, de Physique des Matériaux et de Cosmochimie, IMPMC, 75005 Paris, France

Abstract

The development of field-effect transistor-based (FET-based) non-volatile optoelectronic memories is vital towards innovations necessary to improve our computer systems. In this work, for the first time, we harnessed the unique charge-trapping and charge-retention properties of solution-processed colloidal nitrogen-doped (N-doped) carbon quantum dots (CQDs) to achieve functional optoelectronic memories programmable by UV illumination with a multilevel writing possibility. In particular, long-lasting memory function can be

[†] Electronic supplementary information (ESI) available: Fig. S1–S7, additional TEM images of the CQDs, Tauc plot of the UV-Visible absorbance of N-doped CQDs, zoom-in view of the PLE spectrum with fittings, time-resolved PL decay trace of N-doped CQDs, normalized PL spectrum of N-doped CQDs under different excitation wavelengths, UV-Visible absorbance and PL spectrum of undoped CQDs, Raman spectrum of the graphene applied in this study, the FET transfer characteristics of the graphene transistor measured in dark and under UV illumination, the FET transfer characteristics of the graphene transistor before and after depositing N-doped CQDs, the FET transfer characteristics of the undoped CQD/graphene transistor under illumination of different power densities, the drain current characteristics of 50 continuous cycles of UV programming and V_G erasing, step-by-step device fabrication procedure.

[*] Corresponding author. Email address: zhuoying.chen@espci.fr (Z. Chen).

achieved thanks to the vast charge trapping sites provided by the N-doped CQDs and the resultant photo-gating effect exercised on the graphene FET. The achieved memory can be erased by a positive gate bias which provides sufficient carriers to remove trapped charges through recombination. This study highlights the possibility to engineer high-performance all-carbon non-volatile FET-based optoelectronic memories through manipulating and coupling the charge-trapping properties of colloidal CQDs and graphene.

Introduction

Innovations on memory components are essential to improve current computer systems, the performance of which is limited by the "von Neumann bottleneck".[1,2] As the developments of Internet of Things (IoT) and big data processing are growing rapidly, there is a high demand for solutions towards ultrahigh-density non-volatile storage. Towards the development of high-performance memories, much research effort is currently being carried out, leading to the achievements on different types of non-volatile memories such as capacitor-type memories, resistor-based memories, and transistor-based memories.[3] A major workhorse of transistor-based memories is composed of floating-gate field-effect transistors (FETs) which show advantages in terms of reliability, scalability, power consumption, non-volatility, and compatibility. They lead to the formation of non-volatile flash memories which are compatible with the complementary metal-oxide-semiconductor (CMOS) technology. In the field of non-volatile flash memories, while silicon-based memories have played a significant role so far,[4] in order to overcome the limits of this technology, further research is still needed to identify new materials and devices alternative to silicon-based memories with new abilities to combine characteristics such as low material cost, absence of heavy-metal toxic elements, adaptability in large-area fabrication, mechanical flexibility, and low-power

consumption.[3,5–8] In particular, optoelectronic memories based on thin-film field-effect transistors (FETs), where the programming and/or erasing are attained by illumination instead of electrical bias, exhibit advantages in terms of power consumption and compatibility with optical circuits and artificial neuromorphic applications.[9–13]

Concerning memory applications, colloidal nanocrystals or nanoparticles have aroused much interest to serve as the charge-trapping or charge-retaining material in non-volatile memory devices.[14–18] This is due either to their rich surface properties providing abundant charge traps[19–24] and/or to the variety of available synthesis/engineering approaches leading to formation of core-shell[21,25] or other nanoparticle/dielectric hybrid structures[7],[21] all of which capable to secure and store charges within the nanoparticle. In addition, many direct-bandgap semiconductor nanoparticles possess strong light absorption coefficients together with absorption/emission properties tunable by synthetic controls either over their dimension or surface properties. Their optical and charge-trapping properties were thus harnessed to achieve FET-based optoelectronic memories over the past years, including attempts applying cadmium and zinc chalcogenide QDs and related core/shell structures,[21,25] rare-earth-doped upconversion fluoride nanocrystals,[26] perovskite quantum dots (QDs),[27] as well as TiO_2 dielectric nanoparticles.[28] For example, by embedding Yb^{3+}/Er^{3+}-co-doped $NaYF_4$ colloidal nanocrystals inside a layer of poly(3-hexylthiophene) within a FET architecture, Zhou et al. demonstrated flexible multilevel optoelectronic memories programable by near-infrared illumination at λ = 980 nm.[26] Nevertheless, rare-earth materials are not sustainable and their low absorption coefficient limits the responsivity of the device. Other similar examples, programmable by visible illumination, were also demonstrated by organic conjugated molecules and polymers.[29,30] Yet, typically, a relatively large lateral source-drain bias (e.g. > 10 V) is necessary for their programming. In addition to optoelectronic memories that utilize visible illumination, ultraviolet (UV)-triggered memories can exhibit advantages avoiding

interference from solar irradiation and indoor lighting.[31] Towards this direction, Han et al. sandwiched charge-trapping CdSe/ZnS core-shell QDs between dielectric layers to achieve flexible UV-controlled FET-based photonic memories.[21] Star et al. applied CVD-grown carbon nanotubes for charge storage in a polymer thin film FET leading to UV-writable optoelectronic memories.[7] On both examples, besides the source-drain voltage, an important gate bias is also necessary to work together with the UV illumination to achieve programming. Recently, Sun et al. decorated the surface of graphene FETs by nitrogen-doped-TiO_2 nanocrystals to achieve highly promising UV-writable multilevel optoelectronic memories which exhibit negligible current loss ten hours after UV programming.[28] The synthesis of such nanocrystals requires nevertheless flammable and dangerous precursor (titanium (IV) butoxide) due to its high sensitivity to air and moisture. Towards the further development of this field, alternative solution-processed material candidates synthesized from environmentally benign and/or biosourceable reactants with earth-abundant compositions can potentially lead to further progresses.

To this aim, colloidal carbon quantum dots (CQDs),[32–34] highly luminescent nanoparticles of carbon which is one of the most abundant elements in our planet, could be excellent candidates. They can be readily synthesized in water by various bio-sourced materials such as citric acid,[35] orange peels,[36] water hyacinth leaves,[37] pomegranate[38] under relatively mild synthesis temperature (≤ 200 °C) by hydrothermal, solvothermal or microwave routes, giving nanoparticles with dimensions ranging from a few to a few tens of nanometers. Instead of being controlled by the nanoparticle dimension, their optical properties are controlled by their rich surface chemical groups and dopants which can be tuned from the synthetic routes and the choice of reactants.[39–41] Attracted by their favorable properties such as high optical absorbance and fluorescence, chemical stability, biocompatibility, and low toxicity,[42,43] previous works have successfully applied them in

bio-imaging,[44] drug delivery,[45] photocatalytic conversion,[46] and photovoltaic devices.[47–49] Towards FET-base memories, Zhang et al. has embedded CQDs inside the active layer of polyvinyl pyrrolidone (PPV)-based FET.[50] Nevertheless, such CQD/PPV FET-memories are not optically enable and the programming of which necessitates a high electrical bias of 60 V. To our best knowledge, there is not yet any report of applying colloidal CQDs in optically-enabled optoelectronic memories.

Herein, for the first time, we harnessed the unique charge-trapping and retention properties of solution-processed nitrogen-doped (N-doped) CQDs to achieve functional UV-enable optoelectronic memories with multilevel writing possibilities. These memories are achieved by exploiting the optical and charging-trapping properties of N-doped CQDs to result in a strong photo-gating effect on graphene FETs. After UV-programming, prolonged charge retention can be obtained exhibiting > 96 % of its initial programmed photocurrent value for a period of ten hours. Such a programmed state can be subsequently erased by a positive gate bias. Together with their facile colloidal synthesis, abundant nature, environmental-friendly compositions, and their excellent memory functionalities, these fully carbon-base non-volatile optoelectronic memories thus provide bright perspectives for the further development of this field.

Experimental

Synthesis of colloidal CQDs. N-doped CQDs were synthesized by a previously reported hydrothermal route.[42] Citric acid (1.0507 g) and ethylenediamine (EDA, 335 µL) was dissolved in 10 mL of deionized (DI) water under vigorous stirring for 30 minutes. The resultant precursor solution was poured into a poly(tetrafluoroethylene) (PTFE)-lined autoclave. After sealing the autoclave, it was placed in an oven at 200 °C for 5 hours. The autoclave was then allowed to naturally cool down to room temperature. The resulting product was a transparent brown-color solution containing CQDs. To purify these CQDs,

dialysis was performed in 2K molecular-weight cut off (MWCO) dialysis cassettes in DI water for 48 hours. For the purpose of comparison, CQDs without nitrogen doping (referred below as "undoped CQDs") were also synthesized according to a previously published procedure.[42] Their synthesis and purification procedures were identical to those stated above on N-doped CQDs except that the N-source, amine (EDA), was not added into the reaction.

Fabrication of CQDs/graphene FET-based optoelectronic memories. CVD-grown monolayer graphene on copper (Cu) foils was obtained from Graphenea Semiconductor SLU. It is then transferred by a method established previously[51] onto heavily *p*-doped Si substrates on which a 300-nm-thick thermal SiO_2 layer as grown as the gate dielectrics. To perform the graphene transfer, poly(methyl methacrylate) (PMMA) was first dissolved in butyl-acetate with a concentration of 40 mg/mL. This PMMA solution was then spun onto the graphene/Cu sample at a spin speed of 2000 rpm for 120 seconds followed by solvent drying at 80 °C for 30 minutes. PMMA-protected graphene/Cu foil was then cut into a desired dimension, large enough to build the FETs mentioned below. They were then carefully placed onto the surface of an etchant formed by 10 wt% of $FeCl_3$ aqueous solution in order to dissolve entirely the Cu foil, leaving the PMMA-protected graphene film floating on the solution's surface. The PMMA/graphene layer was then transferred (with the help of a glass slide) onto three different clean DI-water baths to remove residual etchant for a duration of 10 minutes in each bath. A thoroughly cleaned Si/SiO_2(300 nm) substrate was then dipped into the last water bath to pick up the floating PMMA/graphene layer, resulting in a smooth film on the Si/SiO_2 surface. This sample was then allowed for a > 12-hour heat treatment at 150 °C to promote graphene adhesion onto the substrate. After cooled down to room temperature, the PMMA layer of the sample was removed by acetone rinsing. After graphene transfer, gold source and drain electrodes were then thermally evaporated through a shadow mask onto the graphene layer, defining a conductive channel with a channel width (W) and length (L) dimension of

W = 3 mm and L = 0.25 mm. A drop (about 36 µL) of CQD DI-water solution with a concentration of about 12 mg/ml was then drop-casted onto the surface of graphene FET followed by drying off the solvent in air. A step-by-step device fabrication procedure together with images is described in the supporting information.

Material and device characterization methods. Transmission electron microscopy (TEM) characterizations were performed by a JEOL 2010 TEM microscope operated at 200 kV. UV-Visible absorbance measurements were performed by a JASCO V770 UV-Vis spectrometer. Excitation-dependent photoluminescence and photoluminescence excitation (PLE) spectra of N-doped CQD solutions were obtained by an Edinburgh Instruments FLS900 Fluorescence spectrometer. Fourier-transform infrared (FT-IR) spectroscopy was measured on CQDs by a PerkinElmer Spectrum Two instrument in an attenuated total reflection (ATR) infrared mode. The Raman spectrum of CQDs was obtained by an Anton Paar Cora 5001 Raman spectrometer with a λ = 785 nm laser. Atomic force microscopy (AFM) characterizations were performed by a Bruker Dimension Icon atomic force microscope in tapping mode. X-ray diffraction (XRD) spectrum was measured on CQDs deposited onto a glass substrate by a PANalytical X'Pert X-ray diffractometer (with Cu-K_α radiation). X-ray photoelectron spectroscopy (XPS) measurements were performed by a SPECS photoelectron spectroscopy system with a mono X-Ray source Al Kα excitation (1486.6 eV). Graphene FET (before CQD deposition) and CQD-decorated graphene FET-base memories were placed in a probe-station in vacuum (with a transparent top window allowing illumination when necessary) where their current/voltage and current-time characteristics were measured by a computer-controlled Keithley 2634 source measurement unit (SMU). To program the memories under test, an UV LED lamp (λ = 365 nm) from Ocean Optics with a fiber-coupled output was shed onto the device through the top window. To measure the transfer characteristics, light illumination at different irradiance was kept for one minute before measurement.

Results and discussion

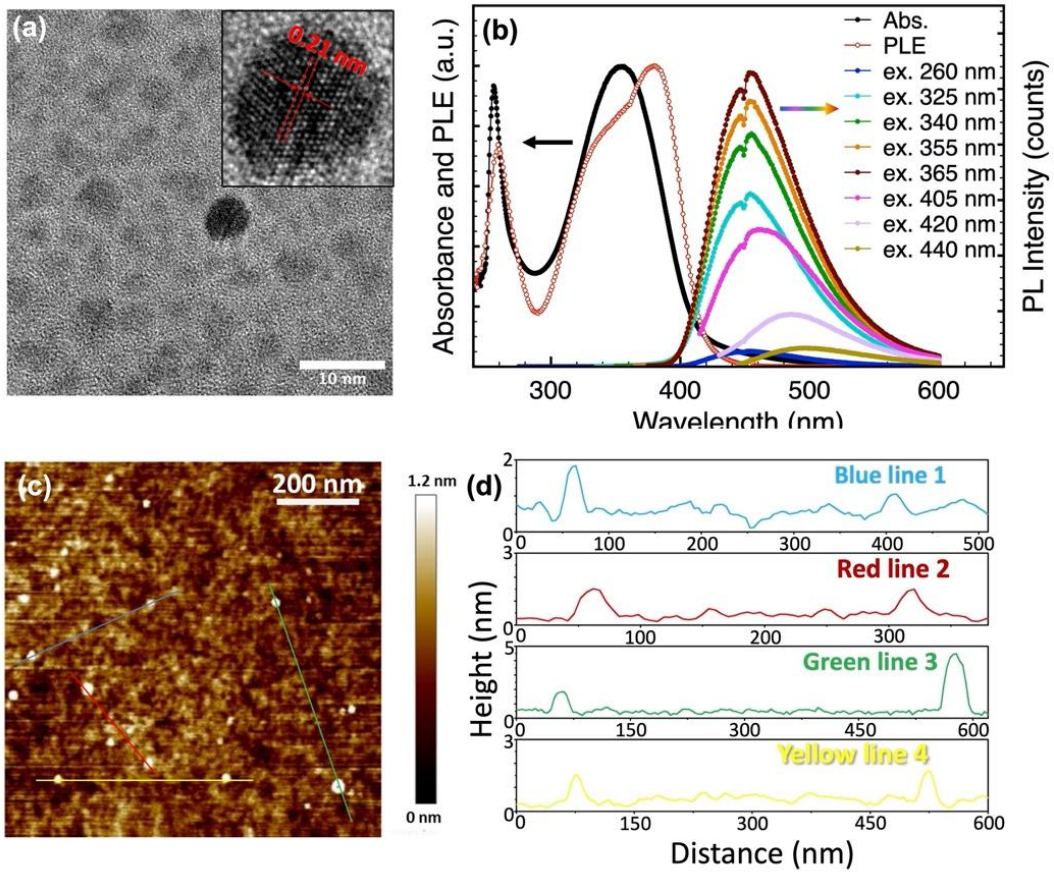

Figure 1. (a) TEM image of N-doped CQDs. The inset is the zoom-in view of the HRTEM image of a N-doped CQD. (b) UV-Visible absorbance, photoluminescence excitation (PLE) and excitation wavelength dependent photoluminescence spectra of the N-doped CQDs in water. (c) AFM image of N-doped CQDs deposited onto a clean Si substrate and (e) the height profiles of the four different lines shown in (c).

The N-doped CQDs under study were synthesized by a reported hydrothermal route with mild synthesis temperature (200 °C) by condensing citric acid together with EDA.[42] TEM images of as-synthesized N-doped CQDs exhibit nanoparticles with a diameter mainly between 2 - 10 nm (Fig. 1(a)). When characterized by high-resolution TEM (HRTEM), some

of them exhibit clear lattice fringes as the one shown in the inset of Fig. 1(a)), where a 0.21-nm interplane distance can be measured corresponding well to the (100) plane distance in graphitized carbon (JCPDS no. 41-1487). When deposited onto a clean Si substrate, these N-doped CQDs reveal a typical height of 2 - 5 nm by AFM characterizations (Fig. 1(c) and (d)), confirming the dimension of the nanoparticles. Additional TEM and AFM images can be found in the supporting information (Fig. S1). In terms of optical properties, N-doped CQDs exhibit two major absorption peaks in the UV spectrum with one located at $\lambda \approx 256$ nm and another strong and broad peak located at $\lambda \approx 356$ nm (Fig. 1(b)). According to previous assignments on similar carbon or graphene quantum dots,[41,52,53] the high-energy absorbance band corresponds to π-π^* transitions in the sp^2 carbon core while the low-energy broad absorbance band contains multiple contributions from both n-π^* transitions (e.g. n_{O2p}-π^* and n_{N2p}- π^*) and π-π^* charge transfer transitions (between the inner and the outer part of the sp^2 domains). Analyzing the on-set of optical absorption by a Tauc plot allows us to determine the optical bandgap as ~ 3.1eV (Fig. S2(a), supporting information). The obtained PLE spectrum is in agreement with the absorbance with a more resolved view on the transitions contributing to the photoluminescence (PL) (fitting on the broad peak shown in Fig. S2(b),). A peak PL intensity was observed when the excitation wavelength is at ~ 380 nm, presumably corresponding to n-π^* transitions which was considered as the major radiative decay pathway for CQDs. Strong blue photoluminescence can be observed when these N-doped CQDs are excited at different wavelengths (Fig. 1(b)). Under an excitation wavelength ($\lambda_{ex.}$) of 405 nm, time-resolved PL trace reveals a bi-exponential decay behavior with an average PL lifetime of about 3.4 ns (Fig. S2(c)), which is in agreement with previous works[54,55] on this type of CQDs. Near identical PL peak shape was observed at different λ_{ex} when it is shorter than ~ 400 nm (Fig. S3(d)). At a longer λ_{ex}, the PL spectrum starts to red-shift with a significant reduced intensity likely due to the increased contribution of the

surface states in the PL[41] and the limited absorbance at these wavelengths. The photoluminescence quantum yield (PLQE) of the N-doped CQDs in water was measured to be about 40% under λ_{ex} = 365 nm. The presence of EDA in the reactants of the present synthesis leads to the formation of N-doping, which was found to contribute to a higher PLQE in comparison to CQDs synthesized without EDA.[42] For the purpose of comparison in the memory devices which will be discussed below, undoped CQDs (without any nitrogen-containing compounds in the reactants) were also synthesized. Coherent with the absence of heteroatom doping, the UV-Vis absorbance of undoped CQDs exhibited a strong π-π* transition band and a very weak low-energy broad absorption band which could be assigned as n-π* and π-π* charge transfer transitions (Fig. S3). By comparison to N-doped CQDs, a much-diminished PL was observed on undoped CQDs at λ_{ex} = 365 nm (Fig. S3) with a very small PLQE reaching only about 1 %. This is likely due to both the absence of the nitrogen doping and the very small absorption coefficient at this λ_{ex}.

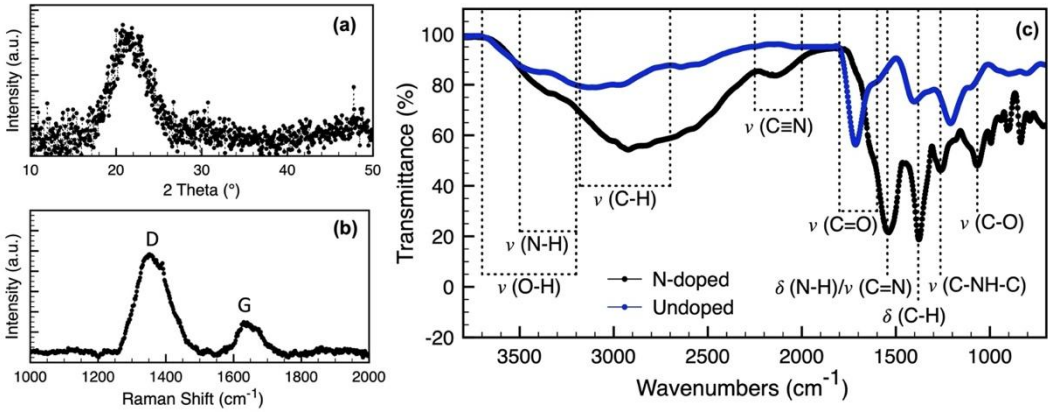

Figure 2. (a) XRD spectrum of as-synthesized N-doped CQDs. (b) Raman spectrum of N-doped CQD solution in water under laser excitation of λ = 785 nm. (c) FT-IR transmission spectrum of N-doped CQDs (black symbols) in comparison to undoped CQDs (blue symbols).

Both XRD and Raman scattering experiments suggest the presence of a high degree of disordering in the present N-doped CQDs likely due to defects and dopants. The XRD spectrum of the N-doped CQDs shows only a broad diffraction peak at $2\theta \sim 21.5°$ which is at a lower diffraction angle than the (001) diffraction peak expected for crystalline graphite ($2\theta = 26.4°$, JCPDS no. 41-1487) (Fig. 2(a)). This is likely due to the presence of a high disorder alone the C-axis and/or the presence of surface/dopant groups enlarging the interplane distance along this axis. The above analysis is coherent with the Raman spectrum obtained (Fig. 2(b)), where two Raman bands, located at the Raman shift of 1355 cm^{-1} and 1645 cm^{-1}, can be observed and assigned as the D and G bands, respectively. The ratio between these two Raman bands (I_D/I_G), typically considered as an indicator of disorder or defect density and as the ratio between sp^3/sp^2 carbons,[56,57] was measured to be ~ 3.2 on the current sample, suggesting a breakage of the hexagonal symmetry of the graphene due to defects and/or heteroatom dopants. From the obtained I_D/I_G ratio and the laser wavelength, by the relationship proposed by Matthews et al.,[58] we estimated the (average) size of the sp^2 domains of the sample to be about 4 nm, which is coherent with the nanoparticle dimension characterized above. FT-IR spectroscopy was further performed on both the N-doped and undoped CQDs in the present work (Fig. 2(c)). On both samples, different vibrations can be observed and attributed to O-H, C-H, C=O and C-O stretching according to previous reports.[35,59–62] In comparison to undoped CQDs, N-doped CQDs exhibit additional vibrations which can be assigned to C-NH-C asymmetric stretching, N-H bending and/or C=N stretching, and possibly also to the C≡N stretching, confirming the nitrogen-doping in the N-doped CQDs. XPS results confirm well that the present N-CQDs mainly composed of C, N, and O (Fig. 3(a)). The C_{1S} spectrum can be fitted into four peaks centered at 284.5, 286.1, 287.7, and 288.3 eV, which can be attributed to bonds of C-C, C-N, C-O, and C=N/C=O, respectively, according to previous reports on CQDs (Fig. 3(b)).[63] The N_{1S}

spectrum reveals two peaks centered at 399.8 and 401.1 eV, which can be assigned from pyrrolic and graphitic N contributions,[64] respectively (Fig. 3(c)). Finally, the O_{1S} spectrum shows two peaks centered at 531.0 and 532.3 eV, which are attributed to bonds of C=O and C-OH/C-O-C,[63] respectively.

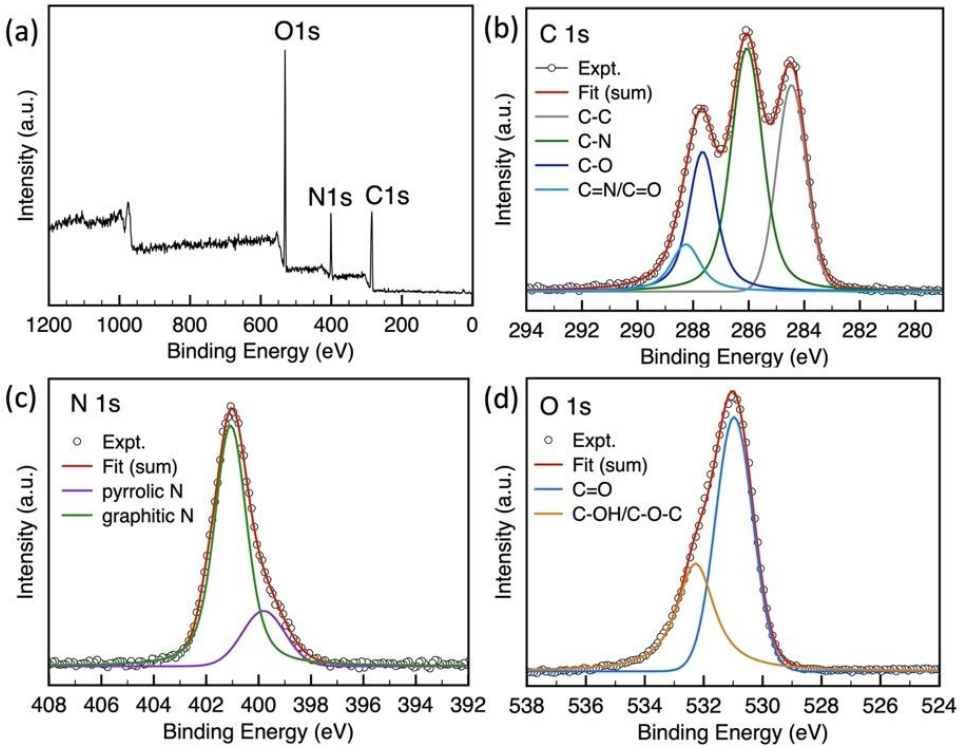

Figure 3. XPS survey scan of N-CQDs drop-casted on Si substrate. (a) XPS full scan spectrum; (b) C_{1S}, (c) N_{1S}, and (d) O_{1S} spectra of the N-CQDs.

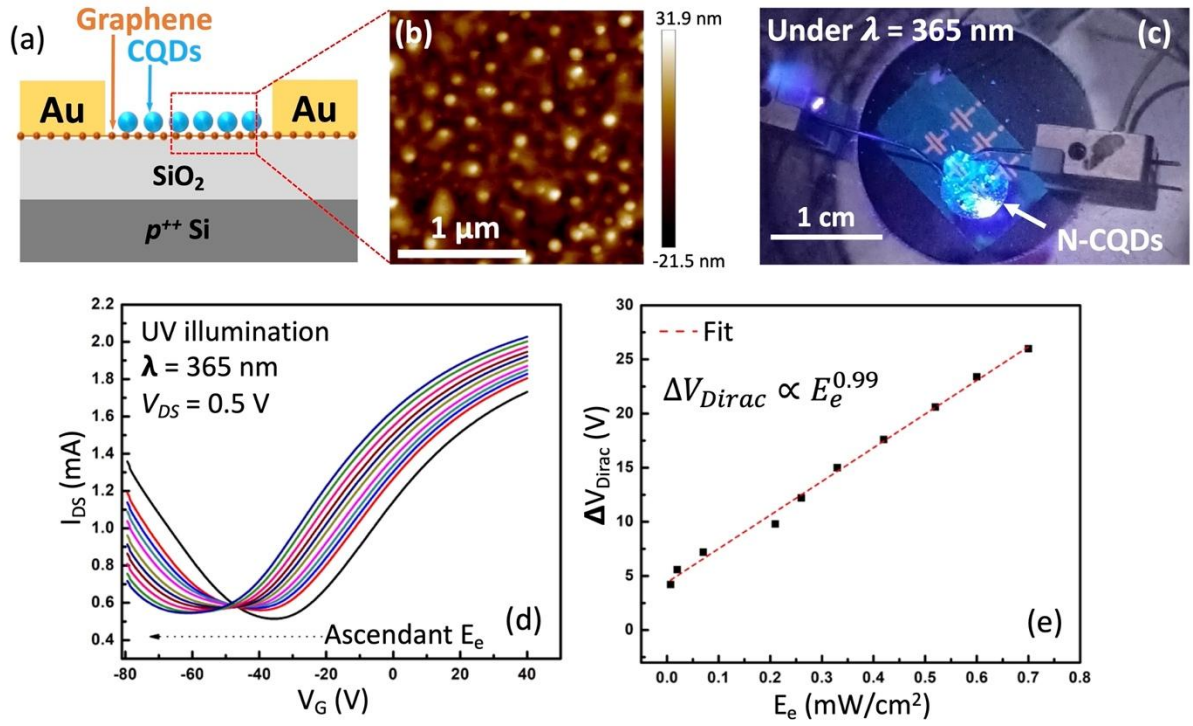

Figure 4. (a) Schematic of the CQD-decorated graphene FET-based optoelectronic memory device structure. (b) AFM image in an area inside the FET channel revealing the decoration of N-doped CQDs on top of the graphene. (c) Image of the CQD-decorated graphene FET sample under test. (d) Transfer characteristics of a N-doped CQD-decorated graphene transistor under UV illumination with a power density (E_e) of 0, 0.007, 0.02, 0.07, 0.21, 0.26, 0.33, 0.42, 0.52, 0.60, 0.70 mW/cm^2. The arrow indicates the shift direction of the transfer characteristics as E_e increases. (e) The shift of the Dirac point voltage (ΔV_{Dirac}) as E_e increases.

The device architecture of the N-doped CQD-decorated graphene FET-based memory is shown in Figure 4(a), where a bottom-gate-top-contact FET structure was applied. The Raman spectrum of the graphene transferred onto the Si/SiO_2 substrate suggested the existence of a single-layer graphene with a similar quality as previously reported CVD-grown graphene (Fig. S4).[65] After depositing N-doped CQDs on the surface of graphene, AFM characterizations were performed inside the FET channel (Fig. 4(b)). While the present AFM

experiment do not have the resolution to resolve an individule CQD, it confirms well their existence on the top surface of the graphene, likely as isolated few-nanoparticle clusters. Fig. 4(c) exhibit a picture of a typical sample under test: Six graphene FETs were fabricated onto the same Si/SiO_2 substrate while the channels of two of them were further decorated by N-CQDs (which exhibits blue fluoresence under UV illumination). Comparing the transfer characteristics of the graphene FET measured in dark before and after depositing N-doped CQDs, a shift of the Dirac point towards negative gate voltages was observed triggered by the deposition of N-doped CQDs (Fig. S5). Such a *n*-type doping behavior is likely due to the interactions between the surface groups and/or defects of the CQDs and the free charges inside the graphene FET channel. Importantly, the decoration of the N-doped CQDs on the graphene FET enables the device a clear photoresponse under UV illumination: A series of UV illuminations (at λ_{ex} = 365 nm) of different power densities (E_a) was shrone from above onto the N-doped-CQD-decorated device. As shown in Fig. 4(d), the UV illumination induced a further shift of the Dirac point of the transfer characteristics towards more negative gate voltages. The magnitude of this shift in Dirac point voltage increases as a larger E_a was applied and the direction of this shift also indicates a further *n*-type doping behavior on the graphene due to the photoexcited N-doped CQDs. This observed UV-sensitivity is clearly different from that observed on graphene FETs without any CQDs, as the same device before depositing N-doped CQDs exhibited negligible shift in terms of Dirac point voltage even under the strongest UV illumination of the present study (Fig. S5). This thus confirms that the observed UV photoresponse should be attributed to the existance of the N-doped CQDs and the interactions between the photoexcitation QDs and the graphene.

The Dirac point voltage shift (ΔV_{Dirac}) measured in the transfer characteristics of the N-doped-CQD/graphene device under different UV illumination power densities (E_a) with reference to the Dirac point measured in dark was plotted in Fig. 4(e). According to previous

works on phototransistors and phototransistor-based memories,[19,65–67] such a ΔV_{Dirac}-E_a relationship can be modeled by power law relationship with $\Delta V_{Dirac} = aE_a^{\beta}$, where α and β are both constants with β typically of values bewteen 0 and 1. A β value much smaller than 1 can, for example, orginate from a saturation of the charge transfer processes between the photo-absorber and the graphene as the illumination irradiance increases due to an increased extent of charge recombination offsetting the increased charge generation. Here, an exceptional near-linear relationship between ΔV_{Dirac} and E_a was observed with β fitted as 0.99 (Fig. 4(e)), indicating a non-saturated photoresponse under the different illumination irradiances of this study. Taken into account of the HOMO and LUMO values measured previously[68–70] on similar N-doped CQDs and the observed shift of ΔV_{Dirac} over E_a, we attribute the physical mechansim behind the current N-doped CQD/graphene device as the photo-gating effect, equivalent to a change in terms of the effective gate voltage due to illumination (Fig. 5). Such a photo-gating effect has been observed in other graphene-based FETs where the graphene was decorated or coupled with another photo-absorber such as PbS quantum dots,[71] a perovskite halide layer,[72,73] black phosphorus nanosheets,[74] and TiO_2 nanocrystals.[19] Here, upon UV absorption, while both types of photoexcited carriers in the N-doped CQDs can be transferred to graphene due to the favorable energy alignments, the observed *n*-type doping behavior upon illumination suggests a more significant electron transfer than hole transfer to the graphene (Fig. 5(a)). This is possible if the photo-generated holes are transferred to the graphene either less efficiently or hindered by traps.[67] As N dopants were found previously to form mid-gap deep hole traps for other types of nanoparticles,[75–77] we thus conjecture that the N-dopants in the current case should serve equally as hole traps. This will be further discussed below when we compare the device behavior with non-N-doped CQDs. As a consequence, the net remaining holes left behind the N-doped CQDs induce more electrons in the graphene channel due to coulomb interactions,

leading to a more negative gate voltage to reach the Dirac point (Fig. 5(b)). The fact that a large and near-unity β was found above in the $\Delta V_{Dirac} - E_a$ relationship suggests the ample availability of hole traps in the N-doped CQDs so that the charge transfer processes are less limited by charge recombinations under the irradiances applied.

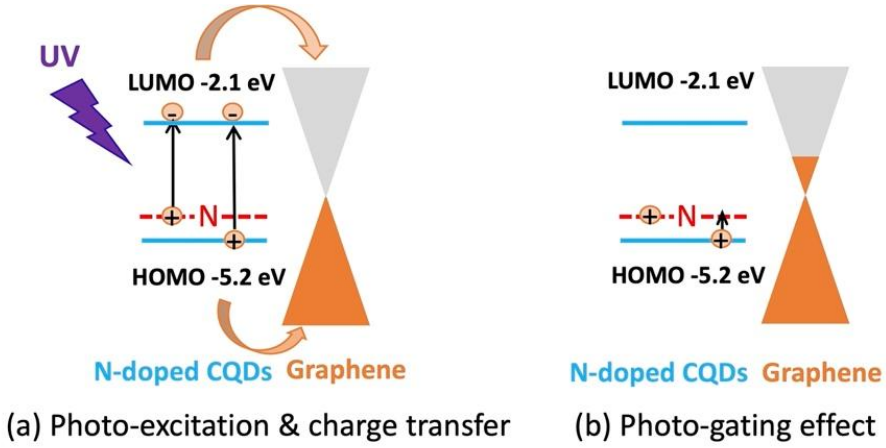

Figure 5. Schematic of (a) the photoexcitation in N-doped CQDs, the subsequent charge transfer processes between CQDs and graphene, and (b) the the photo-gating effect due to the remaining of one type of photo-excited carriers in CQDs.

Coherent with the photo-gating and nitrogen hole-trapping mechanism proposed above, in N-doped-CQD-decorated graphene devices an exceptional charge retaining behavior was oberved (Fig. 6). When the mobility remain unchanged (which is the case in Fig. 4(a)), the Dirac point shift (ΔV_{Dirac}) triggered by UV illumination translates into photocurrents following the relation of $\Delta I_{DS} = \frac{W}{L} C_i \mu \Delta V_{Dirac} V_{DS}$ assuming the FET in the linear regime, where C_i is the capacitance per unit area of the gate dielectric, W and L are respectively the channel width and channel length, I_{DS} and V_{DS} are respectively the source-drain current and the source-drain voltage, and the photocurrent ΔI_{DS} is the change of I_{DS} triggered by illumination by comparison to the $I_{DS,dark}$ measured in dark. The evolution of ΔI_{DS} over time of the N-doped CQD device was monitored at a gate voltage V_G = 0 V and a source-drain

voltage V_{DS} = 0.5 V while a UV light (λ = 365 nm, E_a = 0.7 mW cm^{-2}) was shrone onto the device from the top for a duration of 120 s. Under this illumination, the $\Delta I_{DS}/I_{DS,dark}$ ratio of the current device reach ~ 16%. As shown in Fig. 6(a), a rapid increase of photocurrent was first observed upon UV illumination. Subsequently, after the UV illumination was switched off, the I_{DS} was maintained at nearly the same programmed level with a slight further increasing trend (up to ~ 8%) during the first two hours after switching off the light. Such a slight increase of I_{DS} is likely due to the device instability and/or bias-stress experienced by the device. Beyond this time window, the I_{DS} starts to decrease very slowly, reaching back to 96% of its initial value (i.e. the I_{DS} value right after switching off the light) ten hours after switching off the light. Based on the observed trend of how the I_{DS} decreases over time, extrapolation suggests approximately > 37 % of charge retention can be obtained ten years after switching off the light. Both the rapid increase of I_{DS} during illumination and the subsequent charge retention after removing the illumination are coherent with the mechanism proposed where a large amount of hole traps, likely due to nitrogen-dopants, exist in the N-doped CQDs capable to firmly immobilize photoexcited holes preventing them from recombination and resulting in a long-lasting photo-gating effect (Fig. 6(c)). By comparison to previous literature on similar graphene FET-based memeories coupled with nitrogen-doped TiO_2 nanocrystals,[19] the current charge retention capability is remarkable, maintaining ≥ 100 % of the programmed state (I_{DS}) for 7 hours after switching off the light. In order to probe whether nitrogen dopants are indeed the origins of the hole traps and the observed memory retention, near identical device as mentioned-above was fabricated except that undoped CQDs were applied to decorate the graphene in this case. The tranfer characterisitcs of the undoped CQD/graphene FET under UV illumination at λ_{ex} = 365 nm of different power densities are shown in Fig. S6. In comparison to N-doped CQD device, under an illumination of λ_{ex} = 365 nm and E_a = 0.7 mW cm^{-2}, the $\Delta I_{DS}/I_{DS,dark}$ ratio and the photoresponsivity of the

undoped device are significantly smaller, reaching only ~ 1.3 %. The evolution of ΔI_{DS} over time of the undoped device was monitored the same way as the N-doped device discussed above (Fig. 6(b)), exhibiting a very different behavoir. Notably, in the undoped CQD device, the photocurrent decreases progressively down to less than 30 % of the highest level within only about a thousand seconds after switching off the light. In another word, in undoped devices, the capability of light-induced charge retention is rather poor, resulting in a more than 70% of loss of programmed state within a thousand seconds (*i.e.* ~ half an hour) after memory writing. Indeed, as shown in the FT-IR spectrum, the current updoped CQDs also have rich chemical groups (e. g. O-H, C-H, C=O and C-O groups) likely mostly on the surface. Even without nitrous carbon groups, in undoped CQDs these surface groups and/or defects may also serve as traps for the photoexcited carriers leading to the observed photoresponse, which is coherent with the non-instantenous decay of the photoresponse after switching of the UV. Nevertheless, in the absence of deep traps capable of retaining charges firmly, the photo-gating effect diminishs rather rapidly after switching off the illuminatin due to carrier recombination (Fig. 6(d)). The comparison of the photocurrent (ΔI_{DS}) evolution over time upon and after UV illumination between the N-doped and the undoped device indirectly confirms the vital role of nitrogen dopants towards a long-lasting non-volatile memory function.

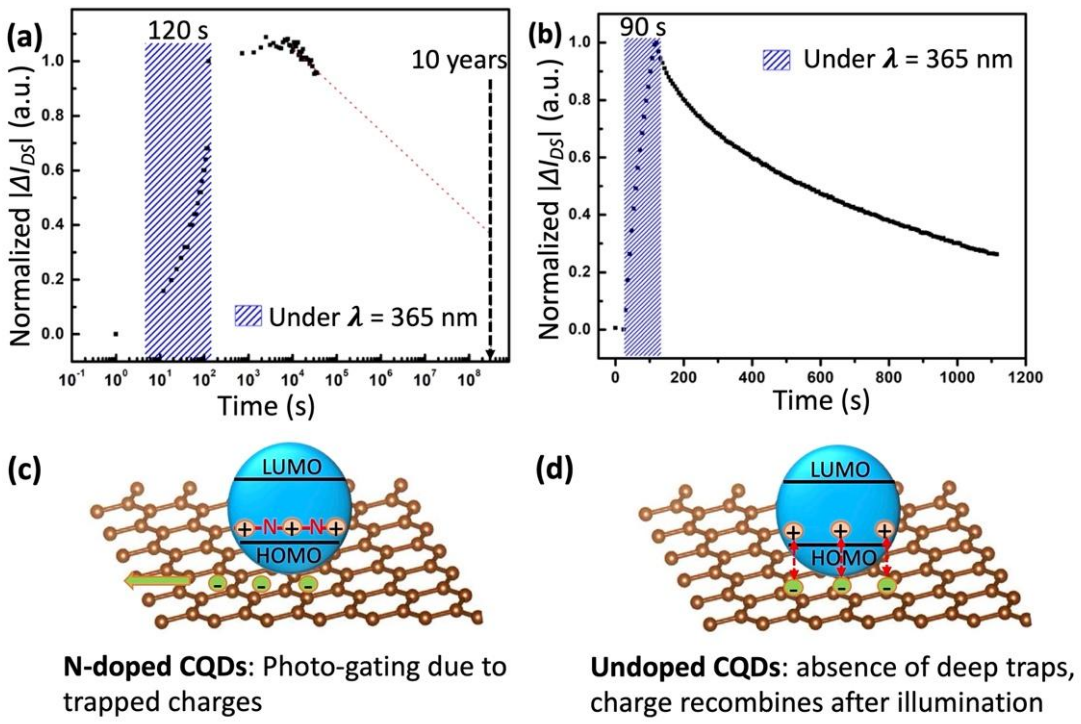

Figure 6. (a) The photoresponse to UV illumination (λ = 365 nm, E_a = 0.7 mW cm^{-2}) in terms of the change of source-drain current I_{DS} by comparison to I_{dark} of a graphene device decorated by N-doped CQDs. The dotted line represents the linear extrapolation of I_{DS} based on the trend observed. (b) The photoresponse to the same UV illumination as (a) of a graphene device decorated by undoped-CQDs. The photocurrents shown in (a) and (b) were measured by fixing V_G = 0 V and V_{DS} = 0.5 V. (c) The schematic corresponding to the situation shown in (a) where holes are trapped and storaged in N-doped CQDs (blue spheres) inducing more electrons in the graphene FET channel by the photo-gating effect. Red lines inside the bandgap represents hole traps likely due to the nitrogen dopants. (d) The schematic corresponding to the situation shown in (b) where undoped CQDs were not able to trap and storage firmly holes which recombines subsequently with the electrons in the graphene after UV illumination.

Consistent with the nitrogen-induced hole-trapping and photo-gating mechanisms proposed above, the achieved memory in the N-doped CQD device after UV programming can be successfully erased by a positive gate voltage applied. Fig. 7(a) exhibits five complete UV-writing and V_G-erasing cycles, where the I_{DS} of the device (measured at V_G = 0 V and V_{DS} = 0.5 V) was first increased to a high level thanks to a UV illumination (λ = 365 nm, E_a = 0.7 mW cm^{-2}) for a duration of 30 seconds. Then a positive gate voltage of +50 V was applied on the device for another duration of 30 seconds, resulting in a drop of I_{DS} back to a level very close to its initial value before UV programming. The characteristics of 50 complete UV-writing and V_G-erasing cycles are shown in Fig. S7, exhibiting globally good reproducibility of the programming and erasing process. The schematic proposing the erasing process is shown in Fig. 7(b). Under a large positive gate voltage, strong electron accumulation is resulted in the FET channel and the Fermi level of the graphene is raised. A large number of electrons can thus be transferred back from the graphene to the N-doped CQDs leading to charge recombination and programmed state erasing. Towards a better applicability of these memory devices, one can expect to apply a lower gate voltage necessary to perform the erasing by strategies such as the application of a thinner SiO_2 gate oxide, or a higher-k gate dielectric material, or ionic gating.

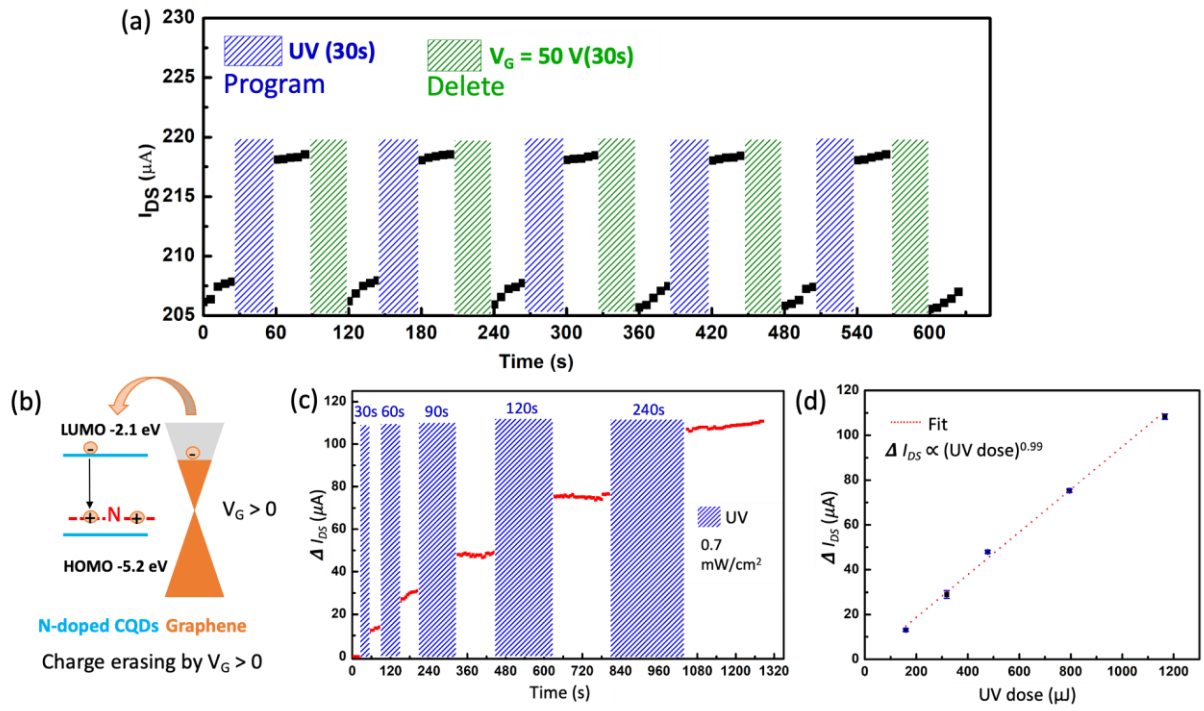

Figure 7. (a) The evolution of I_{DS} of a N-doped CQD device upon five continuous cycles of a 30-second UV (λ = 365 nm, E_a = 0.7 mW cm^{-2}) programming and an erasing operation by the application of a +50 V gate voltage (V_G). The characteristics upon 50 continuous programming/erasing cycles are shown in the supporting information. (b) Schematic of the memory erasing mechanism on a N-doped CQD device when a positive gate voltage is applied. (c) Instant photocurrent response of the N-doped CQD device to UV illumination (λ = 365 nm, E_a = 0.7 mW cm^{-2}) with different durations. Both The data shown in (a) and (c) were measured by setting V_G = 0 V and V_{DS} = 0.5 V. (d) The evolution of ΔI_{DS} over different incident UV doses extracted from (c). The red dotted line represents the numerical fitting.

Finally, by modifying the dose of the illumination, we demonstrate that multilevel memory retention can be achieved in the current N-doped CQD devices. As shown in Fig. 7(c), upon receiving three consecutive UV illuminations of the same irradiance (0.7 mW cm^{-2}) but a different illumination duration, the device exhibits a stepwise increase of photocurrent (ΔI_{DS}). Such a distinctive multilevel writing capability can be potentially

translated into memory applications for multi-bit information storage. Taking into account the illumination duration, the power density, and the active channel area of the device, one can calculate the illumination dose in the unit of joule. The dose information was then plotted together with the corresponding photocurrent shown in Fig. 7(d). A nearly linear relationship can be obtained between the measured photocurrent and the illumination dose, which is in agreement with the observed ΔV_{Dirac}-E_a behavoir shown in Fig. 4(e) where the dose was modified by changing the power density of the illumination instead of duration.

Conclusion

FET-based non-volatile multilevel optoelectronic memory is demonstrated by coupling graphene transistors and colloidal N-doped CQDs. The hybrid N-doped CQD/graphene memory devices are sensitive to UV photons such as those with a wavelength of 365 nm. Upon UV illumination, the photo-excited N-doped CQDs result in a more significant transfer of electrons than holes from the CQDs to the graphene, likely due to the photo-excited holes being trapped by the nitrogen dopants of the N-doped CQDs. This leads to a prominent photo-gating effect and a *n*-type doping of the graphene FET. In comparison to undoped CQD/graphene devices where only poor charge retention was observed, N-doped CQD devices exhibited long-lasting light-induced memory behavior which highlights the vital role of the nitrogen dopant-induced charge trapping in the functioning of the memory device. On N-doped CQD devices, multilevel memory functions are demonstrated triggered by UV illumination of a controlled dose under a gate bias of 0 V. After UV programming, the drain current of the N-doped CQD/graphene FET memory can be maintained at a high level (to > 96 % of the I_{DS} value right after switching off the light) for ten hours. Such a strong charge-retention capability and memory function can be erased by an external positive gate bias, by

which strong electron accumulation was induced in the graphene FET leading to the removal of the trapped hole-retention in the N-doped CQDs through charge recombination. Taking into account the abundant availability of carbon elements, the facile solution synthesis routes and the demonstrated long-lasting non-volatile memory function, these fully carbon-based CQD/graphene FET devices provide interesting perspectives for the further development of transistor-based optoelectronic memories.

Acknowledgements

M. Chaudhary received PhD thesis funding from the European Union's Horizon 2020 research and innovation program under the Marie Skłodowska-Curie grant agreement No 754387. C. Xin, Z. Hu, D. Zhang acknowledge the China Scholarship Council (CSC) for PhD thesis funding.

Conflict of Interest

The authors declare no conflict of interest.

References:

[1] Nonvolatile Memories— Materials, Devices and Applications, *Chemical & Engineering News Archive* **2013**, *91*, 35.

[2] Wm. A. Wulf, S. A. McKee, *ACM SIGARCH Computer Architecture News* **1995**, *23*, 20.

[3] S. T. Han, Y. Zhou, V. A. L. Roy, *Towards the development of flexible non-volatile memories*, Vol. 25, Wiley-VCH Verlag, **2013**, pp. 5425–5449.

[4] M. Grajower, N. Mazurski, J. Shappir, U. Levy, *Laser Photon Rev* **2018**, *12*, 1700190.

[5] Z. Lv, Y. Wang, J. Chen, J. Wang, Y. Zhou, S. T. Han, *Semiconductor Quantum Dots for Memories and Neuromorphic Computing Systems*, Vol. 120, American Chemical Society, **2020**, pp. 3941–4006.

[6] Z. Zhu, Y. Guo, Y. Liu, *Application of organic field-effect transistors in memory*, Vol. 4, Royal Society of Chemistry, **2020**, pp. 2845–2862.

[7] A. Star, Y. Lu, K. Bradley, G. Grüner, *Nano Lett* **2004**, *4*, 1587.

[8] Z. Chen, J. Fang, F. Gao, T. J. K. Brenner, K. K. Banger, X. Wang, W. T. S. Huck, H. Sirringhaus, *Org Electron* **2011**, *12*, 461.

[9] Y. Lin, G. Li, P. Yu, E. Ercan, W. Chen, *Journal of the Chinese Chemical Society* **2022**.

[10] C. Rios, M. Stegmaier, P. Hosseini, D. Wang, T. Scherer, C. D. Wright, H. Bhaskaran, W. H. P. Pernice, *Nat Photonics* **2015**, *9*, 725.

[11] Y. Yu, Q. Ma, H. Ling, W. Li, R. Ju, L. Bian, N. Shi, Y. Qian, M. Yi, L. Xie, W. Huang, *Small-Molecule-Based Organic Field-Effect Transistor for Nonvolatile Memory and Artificial Synapse*, Vol. 29, Wiley-VCH Verlag, **2019**.

[12] L. Shao, H. Wang, Y. Yang, Y. He, Y. Tang, H. Fang, J. Zhao, H. Xiao, K. Liang, M. Wei, W. Xu, M. Luo, Q. Wan, W. Hu, T. Gao, Z. Cui, *ACS Appl Mater Interfaces* **2019**, *11*, 12161.

[13] H. Ling, D. A. Koutsouras, S. Kazemzadeh, Y. van de Burgt, F. Yan, P. Gkoupidenis, *Electrolyte-gated transistors for synaptic electronics, neuromorphic computing, and adaptable biointerfacing*, Vol. 7, American Institute of Physics Inc., **2020**.

[14] J. Yang, M. K. Choi, D.-H. Kim, T. Hyeon, *Advanced Materials* **2016**, *28*, 1176.

[15] M. Liu, N. Yazdani, M. Yarema, M. Jansen, V. Wood, E. H. Sargent, *Nat Electron* **2021**, *4*, 548.

[16] C. Li, Y. Vaynzof, G. Lakhwani, G. J. Beirne, J. Wang, N. C. Greenham, *J Appl Phys* **2017**, *121*, 144503.

[17] J. Wang, B. Sun, F. Gao, N. C. Greenham, *physica status solidi (a)* **2010**, *207*, 484.

[18] J. Wang, F. Gao, N. C. Greenham, *Appl Phys Lett* **2010**, *97*, 053301.

[19] Z. Sun, J. Li, C. Liu, S. Yang, F. Yan, *Nano Lett* **2021**, *21*, 723.

[20] A. A. Bakulin, S. Neutzner, H. J. Bakker, L. Ottaviani, D. Barakel, Z. Chen, *ACS Nano* **2013**, *7*, 8771.

[21] S.-T. Han, Y. Zhou, L. Zhou, Y. Yan, L.-B. Huang, W. Wu, V. A. L. Roy, *J Mater Chem C Mater* **2015**, *3*, 3173.

[22] P. Kumari, J. Ko, V. R. Rao, S. Mhaisalkar, W. L. Leong, *IEEE Electron Device Letters* **2020**, *41*, 852.

[23] F. Ambrosio, D. Meggiolaro, E. Mosconi, F. de Angelis, *J Mater Chem A Mater* **2020**, *8*, 6882.

[24] D. Becker-Koch, M. Albaladejo-Siguan, V. Lami, F. Paulus, H. Xiang, Z. Chen, Y. Vaynzof, *Sustain Energy Fuels* **2020**, *4*, 108.

[25] Y. J. Jeong, D.-J. Yun, S. H. Noh, C. E. Park, J. Jang, *ACS Nano* **2018**, *12*, 7701.

[26] Y. Zhou, S.-T. Han, X. Chen, F. Wang, Y.-B. Tang, V. A. L. Roy, *Nat Commun* **2014**, *5*, 4720.

[27] Y. Wang, Z. Lv, J. Chen, Z. Wang, Y. Zhou, L. Zhou, X. Chen, S. T. Han, *Advanced Materials* **2018**, *30*.

[28] Z. Sun, J. Li, C. Liu, S. Yang, F. Yan, *Nano Lett* **2021**, *21*, 723.

[29] Y. Guo, C. Di, S. Ye, X. Sun, J. Zheng, Y. Wen, W. Wu, G. Yu, Y. Liu, *Advanced Materials* **2009**, *21*, 1954.

[30] L. Zhang, T. Wu, Y. Guo, Y. Zhao, X. Sun, Y. Wen, G. Yu, Y. Liu, *Sci Rep* **2013**, *3*, 1080.

[31] L. Peng, L. Hu, X. Fang, *Advanced Materials* **2013**, *25*, 5321.

[32] C. J. Reckmeier, J. Schneider, A. S. Susha, A. L. Rogach, *Opt Express* **2016**, *24*, A312.

[33] L. Cao, K. A. Shiral Fernando, W. Liang, A. Seilkop, L. Monica Veca, Y.-P. Sun, C. E. Bunker, *J Appl Phys* **2019**, *125*, 220903.

[34] Y. Vyas, P. Chundawat, D. Dharmendra, P. B. Punjabi, C. Ameta, *Int J Hydrogen Energy* **2021**, *46*, 37208.

[35] S. Zhu, Q. Meng, L. Wang, J. Zhang, Y. Song, H. Jin, K. Zhang, H. Sun, H. Wang, B. Yang, *Angewandte Chemie* **2013**, *125*, 4045.

[36] X. Hu, Y. Li, Y. Xu, Z. Gan, X. Zou, J. Shi, X. Huang, Z. Li, Y. Li, *Food Chem* **2021**, *339*, 127775.

[37] Y. Vyas, P. Chundawat, D. Dharmendra, A. Jain, P. B. Punjabi, C. Ameta, *Mater Chem Phys* **2022**, *281*, 125921.

[38] Y. Vyas, P. Chundawat, Dharmendra, P. B. Punjabi, C. Ameta, *ChemistrySelect* **2021**, *6*, 8566.

[39] T. Yuan, T. Meng, P. He, Y. Shi, Y. Li, X. Li, L. Fan, S. Yang, *J Mater Chem C Mater* **2019**, *7*, 6820.

[40] K. J. Mintz, Y. Zhou, R. M. Leblanc, *Nanoscale* **2019**, *11*, 4634.

[41] G. Yang, C. Wu, X. Luo, X. Liu, Y. Gao, P. Wu, C. Cai, S. S. Saavedra, *The Journal of Physical Chemistry C* **2018**, *122*, 6483.

[42] S. Zhu, Q. Meng, L. Wang, J. Zhang, Y. Song, H. Jin, K. Zhang, H. Sun, H. Wang, B. Yang, *Angewandte Chemie - International Edition* **2013**, *52*, 3953.

[43] F. Yan, Z. Sun, H. Zhang, X. Sun, Y. Jiang, Z. Bai, *The fluorescence mechanism of carbon dots, and methods for tuning their emission color: a review*, Vol. 186, Springer-Verlag Wien, **2019**.

[44] I. J. Gomez, B. Arnaiz, M. Cacioppo, F. Arcudi, M. Prato, *J Mater Chem B* **2018**, *6*, 5540.

[45] A. Nair, J. T. Haponiuk, S. Thomas, S. Gopi, *Biomedicine & Pharmacotherapy* **2020**, *132*, 110834.

[46] W. Zhang, Y. Zhou, C. Dong, B. Shen, M. Xing, J. Zhang, *Research on Chemical Intermediates* **2018**, *44*, 4797.

[47] P. Huang, S. Xu, M. Zhang, W. Zhong, Z. Xiao, Y. Luo, *Opt Mater (Amst)* **2020**, *110*, 110535.

[48] S. Wang, Y. Zhu, B. Liu, C. Wang, R. Ma, *J Mater Chem A Mater* **2019**, *7*, 5353.

[49] Z. Li, F. Wang, C. Liu, F. Gao, L. Shen, W. Guo, *J Mater Chem A Mater* **2019**, *7*, 22359.

[50] W. Zhang, X. Guo, J. Yin, J. Yang, *Electronics (Basel)* **2020**, *9*, 753.

[51] J. W. Suk, A. Kitt, C. W. Magnuson, Y. Hao, S. Ahmed, J. An, A. K. Swan, B. B. Goldberg, R. S. Ruoff, *ACS Nano* **2011**, *5*, 6916.

[52] W. Kwon, S. Do, J.-H. Kim, M. Seok Jeong, S.-W. Rhee, *Sci Rep* **2015**, *5*, 12604.

[53] F. A. Permatasari, A. H. Aimon, F. Iskandar, T. Ogi, K. Okuyama, *Sci Rep* **2016**, *6*, 21042.

[54] L. Wang, W. Li, L. Yin, Y. Liu, H. Guo, J. Lai, Y. Han, G. Li, M. Li, J. Zhang, R. Vajtai, P. M. Ajayan, M. Wu, *Sci Adv* **2020**, *6*.

[55] J. Guo, H. Li, L. Ling, G. Li, R. Cheng, X. Lu, A.-Q. Xie, Q. Li, C.-F. Wang, S. Chen, *ACS Sustain Chem Eng* **2020**, *8*, 1566.

[56] H. Li, Z. Kang, Y. Liu, S.-T. Lee, *J Mater Chem* **2012**, *22*, 24230.

[57] H. Ming, Z. Ma, Y. Liu, K. Pan, H. Yu, F. Wang, Z. Kang, *Dalton Transactions* **2012**, *41*, 9526.

[58] M. J. Matthews, M. A. Pimenta, G. Dresselhaus, M. S. Dresselhaus, M. Endo, *Phys Rev B* **1999**, *59*, R6585.

[59] Q. Zhang, S. Du, F. Tian, X. Long, S. Xie, S. Tang, L. Bao, *Molecules* **2022**, *27*, 4586.

[60] P. Wu, W. Li, Q. Wu, Y. Liu, S. Liu, *RSC Adv* **2017**, *7*, 44144.

[61] J. Zhao, Q. Song, F. Wu, X. Guo, T. Xu, *IOP Conf Ser Earth Environ Sci* **2019**, *344*, 012068.

[62] C. Liu, L. Bao, B. Tang, J.-Y. Zhao, Z.-L. Zhang, L.-H. Xiong, J. Hu, L.-L. Wu, D.-W. Pang, *Small* **2016**, *12*, 4702.

[63] Q. Yang, J. Duan, W. Yang, X. Li, J. Mo, P. Yang, Q. Tang, *Appl Surf Sci* **2018**, *434*, 1079.

[64] A. R. Nallayagari, E. Sgreccia, R. Pizzoferrato, M. Cabibbo, S. Kaciulis, E. Bolli, L. Pasquini, P. Knauth, M. L. Di Vona, *J Nanostructure Chem* **2022**, *12*, 565.

[65] J. Wen, C. Yan, Z. Sun, *Adv Electron Mater* **2020**, *6*, 2000031.

[66] H. Fang, W. Hu, *Advanced Science* **2017**, *4*, 1700323.

[67] Z. Sun, Z. Liu, J. Li, G. Tai, S.-P. Lau, F. Yan, *Advanced Materials* **2012**, *24*, 5878.

[68] K. M. Omer, D. I. Tofiq, A. Q. Hassan, *Microchimica Acta* **2018**, *185*, 466.

[69] Y. Zhao, J. Duan, B. He, Z. Jiao, Q. Tang, *Electrochim Acta* **2018**, *282*, 255.

[70] G. Yang, C. Wu, X. Luo, X. Liu, Y. Gao, P. Wu, C. Cai, S. S. Saavedra, *The Journal of Physical Chemistry C* **2018**, *122*, 6483.

[71] Z. Sun, Z. Liu, J. Li, G. A. Tai, S. P. Lau, F. Yan, *Advanced Materials* **2012**, *24*, 5878.

[72] M. Serhan, M. Sprowls, D. Jackemeyer, M. Long, I. D. Perez, W. Maret, N. Tao, E. Forzani, In *AIChE Annual Meeting, Conference Proceedings*, American Institute of Chemical Engineers, **2019**.

[73] Z. Sun, L. Aigouy, Z. Chen, *Nanoscale* **2016**, *8*, 7377.

[74] G. Zhou, Z. Li, Y. Ge, H. Zhang, Z. Sun, *Nanoscale Adv* **2020**, *2*, 1059.

[75] D. Li, P. Jing, L. Sun, Y. An, X. Shan, X. Lu, D. Zhou, D. Han, D. Shen, Y. Zhai, S. Qu, R. Zbořil, A. L. Rogach, *Advanced Materials* **2018**, *30*.

[76] L. Jiang, H. Ding, M. Xu, X. Hu, S. Li, M. Zhang, Q. Zhang, Q. Wang, S. Lu, Y. Tian, H. Bi, *Small* **2020**, *16*.

[77] N. A. A. Nazri, N. H. Azeman, Y. Luo, A. A. A Bakar, *Carbon quantum dots for optical sensor applications: A review*, Vol. 139, Elsevier Ltd, **2021**.

Table of Contents (TOC) text and graphic

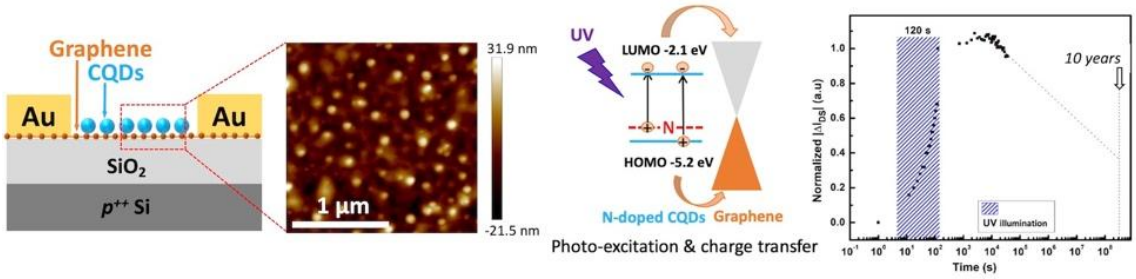

Hybrid colloidal nitrogen-doped carbon quantum dot/graphene optoelectronic memories are fabricated. UV-triggered multilevel memory functions are demonstrated together with exceptional charge retention capability. Ten hours after programming, the drain current of the memory device still remains > 96 % of its initial current value.